Separation of deformable particles in deterministic lateral displacement devices

Raymond Quek, Duc Vinh Le, and K.-H. Chiam*

*A*STAR Institute of High Performance Computing, 1 Fusionopolis Way #16-16, Singapore 138632, Singapore*

(Received 11 October 2010; revised manuscript received 17 March 2011; published 2 May 2011)

Using numerical simulations, we study the separation of deformable bodies, such as capsules, vesicles, and cells, in deterministic lateral displacement devices, also known as bump arrays. These arrays comprise regular rows of obstacles such as micropillars whose arrangements are shifted between adjacent rows by a fixed amount. We show that, in addition to the zigzag and laterally displaced trajectories that have been observed experimentally, there exists a third type of trajectory which we call dispersive, characterized by seemingly random bumpings off the micropillars. These dispersive trajectories are observed only for large and rigid particles whose diameters are approximately more than half the gap size between micropillars and whose stiffness exceeds approximately 500 MPa. We then map out the regions in phase space, spanned by the row shift, row separation, particle diameter, and particle deformability, in which the different types of trajectories are expected. We also show that, in this phase space, it is possible to transition from zigzag to dispersive trajectories, bypassing lateral displacement. Experimentally, this is undesirable because it limits the ability of the device to sort particles according to size. Finally, we discuss how our numerical simulations may be of use in device prototyping and optimization.

DOI: 10.1103/PhysRevE.83.056301 PACS number(s): 47.55.−t, 47.11.−j, 47.61.−k

I. INTRODUCTION

Deterministic lateral displacement devices, or bump arrays as they are commonly called, are microfluidic devices used to separate particles according to size [1]. They comprise rows of micropillars arranged such that each row of micropillars is shifted laterally from the previous row. A sketch of the arrangement of the micropillars in such a device is shown in Fig. 1. Fluid and particles immersed in the fluid are flowed through this array. Because of the low operating Reynolds number, reported in typical experiments [1] to be around 10^{-3}, the fluid flow is laminar. Particles will therefore follow streamlines as they migrate through the array. If the particles are small, beyond a certain critical diameter to be determined, then they "fit" within the streamlines and will zigzag cyclically through the gaps between micropillars without "bumping" into the shifted downstream micropillars. However, if the particles are larger than the critical diameter, then they do not fit within the streamlines and will be bumped by the shifted downstream micropillars laterally into the adjacent streamlines. Consequently, the movement of large particles through this array is one of lateral displacement, bumping off the micropillars. If a mixture of particles of varying sizes is being flowed through this array, they will be separated and sorted according to size, with the larger particles experiencing lateral displacement and the small particles experiencing no lateral displacement. This principle forms the basis of using the microfluidic device as a sorting device to separate particles according to size. In practice, it is possible to fractionate particles into a wide range of sizes by placing arrays of different amounts of lateral shifts in series. Successful applications of these devices include the fractionation of whole blood components into platelets, red cells, and white cells [2], enrichment of large cells for tissue engineering [3], determination of blood cell size [4], lysing, labeling, and washing of cells [5], etc.

In this article, we describe the use of numerical simulations to study the fluid dynamics of this separation process in more detail. In particular, we focus on the trajectories of deformable particles as they pass through the micropillar array. There have been some theoretical studies of deterministic lateral displacement for rigid particles [6,7], but theoretical studies for deformable particles is not an easy subject to treat theoretically. This is because of the complexity involved in the deformation of particles caused by shearing torques and hydrostatic pressure gradients. Here, we instead rely on numerical simulations to understand these particle-fluid and particle-pillar interactions and how they modify the separation characteristics of the array.

Referring to Fig. 1, the key parameters governing the flow of particles through the array are as follows:

(1) The lateral shift between adjacent rows of micropillars d, which we can express dimensionlessly as $\epsilon \equiv d/\lambda$, where λ is the center-to-center spacing between the micropillars.

(2) The center-to-center distance between adjacent rows of micropillars l, which we can express dimensionlessly as $\beta \equiv l/\lambda$.

(3) The gap size between two adjacent micropillars G, which we can express dimensionlessly as $\eta \equiv G/\phi$, where ϕ is the diameter of the micropillars.

(4) The diameter of the particles D, which we can express dimensionlessly as $\delta \equiv D/G$.

(5) The deformability of the particles, characterized by their stiffness k, which we can express dimensionlessly as $\gamma \equiv (p_0/L)/(k/x^2)$, where p_0 is the pressure differential applied over the length L of the device, and x is a characteristic length scale chosen here to be 20 μm, a characteristic particle diameter. Thus, $\gamma = 0$ corresponds to rigid particles and increasing γ corresponds to increasing deformability. Low values of γ correspond to rigid particles, while increasing γ corresponds to increasing deformability. For example, polystyrene beads with a stiffness of 3 GPa will have $\gamma = 3.79 \times 10^{-12}$, while cells with a characteristic stiffness of 1 kPa will have $\gamma = 1.14 \times 10^{-5}$.

*chiamkh@ihpc.a-star.edu.sg

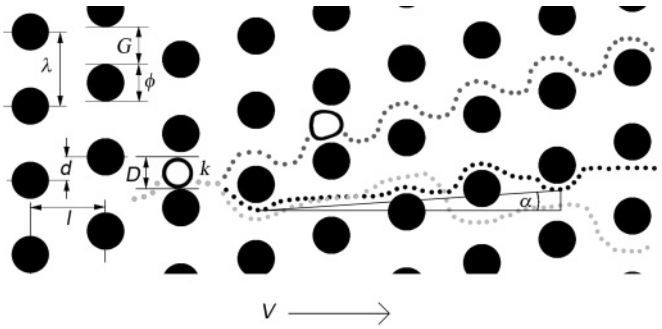

FIG. 1. Sketch of the arrangement of the micropillar array in deterministic lateral displacement devices. The micropillars (whose cross-sectional area is shown here as black filled circles) have diameters ϕ, and are arranged such that the center-to-center distance between two micropillars in a row is λ and the center-to-center distance between two rows of micropillars is l. The gap between two micropillars in a row is $G \equiv \lambda - \phi$, and the lateral shift between two rows is d. Fluid is flown through the array at speed V from left to right, determined by a pressure differential of magnitude p_0. Particles of diameter D and stiffness k are flown through the array. They may be deformed by the flow field as they flow. Some possible trajectories are shown by the series of gray dots. The angular displacement of the particle is denoted by α.

In addition, we assume that our particles are spherical elastic capsules, i.e., the particles are comprised of a Hookean membrane of stiffness k enclosing fluid that has the same properties as the extracellular fluid. Other constitutive models for membranes, such as the Helfrich or Skalak models [8,9], can be used instead. Also, nonspherical shapes (elliptical, biconcave, etc.) can be used instead. We also assume that the micropillars are rigid and have circular cross sections, although other shapes can be used instead. In fact, there have been recent studies to show that performance is improved when triangular posts are used instead [10].

Finally, we note that in our simulations, we will be neglecting particle diffusion, whose effect on separation in these arrays has been studied theoretically [11]. We are interested in the separation of cells and vesicles whose smallest characteristic size is around 1 μm. As discussed in Ref. [2], in typical operating velocities of 10^{-3} m/s, the Péclet number is around 10^3. Hence, advection dominates diffusion and we can safely neglect particle diffusion and broadening of the displacements as the particles move through the array. Hence, the separation process is deterministic. A consequence of this is that, the faster the flow rate, the less broadening due to diffusion, and the performance of the array increases.

In this study, we do not vary the Reynolds number because we expect it to be very close to zero and therefore the flow to be Stokesian. In the experiments, the Reynolds number was estimated to be around 10^{-3} [1]. We found in our simulations that the Reynolds number is around 7×10^{-4}.

The remaining of this article is organized as follows. In Sec. II, we describe the numerical methods used to simulate the fluid flow and deformable particles. In Sec. III, we discuss the results obtained from our simulations and compare them to experimental observations. Finally, in Sec. IV, we present our conclusions.

II. METHODS

Our simulations rely on the immersed boundary method [12]. We have described our numerical implementation of the method elsewhere and will not repeat the details here [13]. In this article, we confine our simulations to two dimensions. In typical experiments [6], the height H of the micropillars is 25μm whereas the diameter D of the particles used varies from 2.3 to 22 μm. Therefore, our two-dimensional simulations will only be valid in those cases when $H \gg D$. Nevertheless, in those cases when $H < D$, we may still expect our simulations to be qualitatively correct.

We define a two-dimensional Cartesian fluid domain Ω that is of length L and width W. In this domain, fluid of viscosity μ and density ρ flows pass an array of immobilized micropillars. A deformable particle is immersed and moves around the fluid. The fluid velocity $\vec{u}(\vec{x},t)$ and pressure $p(\vec{x},t)$ everywhere in the domain are obtained from solving the incompressible Navier-Stokes equation,

$$\rho\left(\frac{\partial \vec{u}}{\partial t} + (\vec{u}\cdot\vec{\nabla})\vec{u}\right) = -\vec{\nabla}p + \mu\Delta\,\vec{u} + \vec{F}, \tag{1}$$

and the continuity equation,

$$\vec{\nabla}\cdot\vec{u} = 0. \tag{2}$$

The inertial terms in Eq. (1) can be neglected because of the low Reynolds number (reported in typical experiments [1] to be around 10^{-3}) but we have kept them in our simulations for completeness. The body force $\vec{F}$ arises from the deformation of the membrane of the moving particle,

$$\vec{F}(\vec{x},t) = \int \vec{f}(s,t)\delta(\vec{x} - \vec{X}(s,t))\,ds, \tag{3}$$

where s is the curvilinear coordinate on the membrane at each material point, $\vec{X}(s,t)$ the position at time t in Cartesian coordinates of the material point whose label is s, $\vec{f}(s,t)$ the force due to the deformation of the moving membrane at material point s, and $\delta(\vec{x} - \vec{X}(s,t))$ the two-dimensional Dirac delta function. The membrane material points are then advected using

$$\frac{d\vec{X}(s,t)}{dt} = \int_\Omega \vec{u}(\vec{x},t)\delta(\vec{x} - \vec{X}(s,t))\,d\vec{x}. \tag{4}$$

In our implementation, the elastic membrane of the particle is represented by a set of N control points $\vec{X}_i(t)$ with $i = 1,\ldots,N$. The elastic forces generating on the membrane are derived from spring forces of the form

$$\vec{f}(\vec{X}_i,t) = -k(\|\vec{X}_{i+1} - \vec{X}_i\| - \Delta s_0)\frac{\vec{X}_i - \vec{X}_{i+1}}{\|\vec{X}_i - \vec{X}_{i+1}\|}, \tag{5}$$

where k is the membrane stiffness and Δs_0 the resting length.

The micropillars are nondeformable and their positions are fixed. Singular forces are applied at the rigid boundaries to impose the no-slip conditions. The singular forces are computed implicitly by solving a small system of equations at each time step [13]. The main advantage of this method is that it imposes the no-slip boundary condition exactly and avoids the need for small time step to maintain stability.

We use a second-order finite difference scheme and make use of the projection method on a marker-and-cell (MAC)

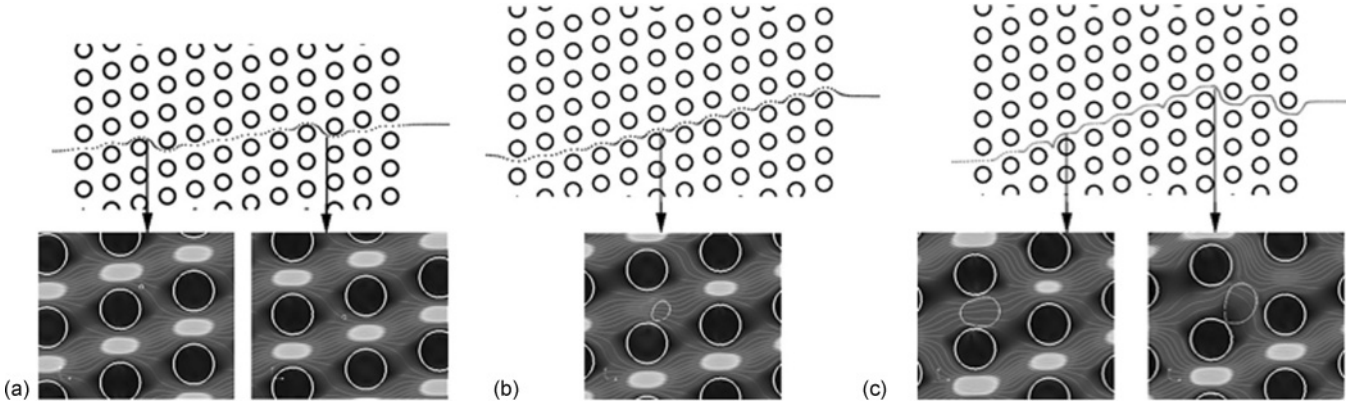

FIG. 2. Plots of the centers of mass of particles migrating through the array. (a) An example of a zigzag trajectory where ($\epsilon = 0.25$, $\beta = 1$, $\eta = 1$, $\delta = 0.2$, $\gamma = 2.066 \times 10^{-10}$). (b) An example of a laterally displaced trajectory where ($\epsilon = 0.25$, $\beta = 1$, $\eta = 1$, $\delta = 0.55$, $\gamma = 2.066 \times 10^{-10}$). (c) An example of a dispersive trajectory where ($\epsilon = 0.33$, $\beta = 1$, $\eta = 1$, $\delta = 0.95$, $\gamma = 2.066 \times 10^{-10}$). Streamline plots at various locations are also plotted for all three types of trajectories. The background color codes are for velocity magnitude, with light colors denoting high magnitudes and dark colors denoting low magnitudes.

grid to solve for Eqs. (1) and (2). In the two-dimensional Cartesian domain ($0 \leqslant x \leqslant L, 0 \leqslant y \leqslant W$), the top ($y = W$) and bottom ($y = 0$) boundaries are periodic. The fluid flows from left ($x = 0$) to right ($x = L$). At the left boundary, the boundary conditions used are $\partial\vec{u}/\partial x|_{x=0} = \vec{0}$ and $p|_{x=0} = p_0$. In this article, we use a value of $p_0 = 5$ kPa, which gives a pressure gradient in our simulations comparable to that of the microdevices used in experiments [1]. At the right boundary, $\partial\vec{u}/\partial x|_{x=L} = \vec{0}$ and $p|_{x=L} = 0$.

III. RESULTS

Using our simulations, we first demonstrate that we can reproduce the two types of trajectories observed experimentally, namely, zigzag and lateral displacement. These different types of trajectories are shown in Figs. 2(a) and 2(b), where we plot the center of mass of the particles at different time points as they migrate through the array. In Fig. 2(a), a zigzag trajectory is shown. The parameters used are $\epsilon = 0.25$, $\beta = 1$, $\eta = 1$, $\delta = 0.2$, and $\gamma = 2.066 \times 10^{-10}$. The value of $\epsilon = 0.25$ means that the arrangement of micropillars is repeated every $1/\epsilon = 4$ rows. Therefore, we can divide the flow through the gap between two adjacent pillars in the same row into $1/\epsilon = 4$ flow streams approximately. If a particle is small enough to fit into one of these streams, i.e., if $\delta < \epsilon = 0.25$, then it can flow pass the $1/\epsilon = 4$ rows without bumping into any of the micropillars. Consequently, the particle will move around the micropillars and exhibit the so-called zigzag mode. We expect the critical diameter δ_c below which zigzag trajectories are observed to be approximately ϵ. We say approximately because the motion of the particles through the fluid in turn distorts the streamlines and so, in practice, the streamlines change with time. Nevertheless, for small δ, i.e., for small particles, this change is not significant. This is evident from the streamline plots in the bottom of panel (a), which show that the streamlines are indeed not significantly perturbed. Therefore, one can in principle solve for the steady-state streamlines in the given geometry in the absence of particles and expect these streamlines to very closely predict the path of particles of small δ. (In these streamline plots, the magnitude of the velocity field is also shown, where light colors denote high speeds and dark colors denote low speeds.)

In contrast, if the particle diameter is larger than the threshold $\delta_c \sim \epsilon$, then the particle does not fit into the flow stream and will be bumped out of the flow stream that it is in by the shifted downstream micropillar, and be laterally displaced to the next adjacent flow stream. Therefore, the trajectory of such large particles comprises a sequence of lateral bumps. An example of such a lateral displacement trajectory is shown in Fig. 2(b). The parameters used are $\epsilon = 0.25$, $\beta = 1$, $\delta = 0.55$, and $\gamma = 2.066 \times 10^{-10}$. In this case, the motion of the particle significantly modifies the streamlines, an example of which is shown in the streamline plot in the bottom of Fig. 2(b). The particle is now large enough to span several streamlines. Owing to the row staggering which displaces the subsequent rows of micropillars upward, most of the streamlines spanned by the particle will be displaced upward rather than downward, leading to the particle to travel in a laterally displaced mode upward.

Both the zigzag and laterally displaced trajectories have been well characterized and studied. Our two-dimensional simulations can reproduce these trajectories. However, in addition to these two types of trajectories, we have also observed a third type of trajectory that comprises mixtures of what look like the former two, i.e., part of the trajectory is of the zigzag type and part of it is of the laterally displaced type. An example is shown in Fig. 2(c). The parameters used are $\epsilon = 0.33$, $\beta = 1$, $\eta = 1$, $\delta = 0.95$, and $\gamma = 2.066 \times 10^{-10}$. This type of trajectory is only seen for large values of $\delta > 0.5$, i.e., the particles are close to "plugging" the interpillar gaps. There is seemingly no pattern as to where the transition from zigzag to lateral displacement, or vice versa, will take place. As a result, particles (of the same size) that are clustered at the inlet tend to become more dispersed at the outlet. Therefore, we call this type of trajectory "dispersive." We will describe this dispersion in more detail later. In the streamline plots of Fig. 2(c), we show, for example, two scenarios of plugging, one of which results in the particle moving upward (laterally

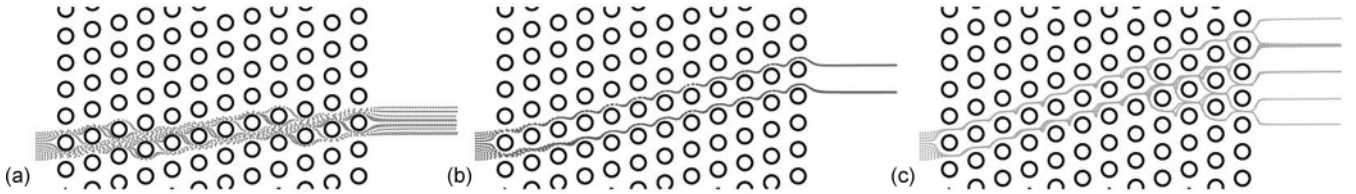

FIG. 3. Dispersion of (a) zigzag, (b) laterally displaced, and (c) dispersive trajectories. The parameters used are as in Fig. 2.

displaced) and the other in the particle moving downward. The latter happens when the plugging action modifies the fluid flow significantly enough that the streamlines bend downward. This can be attributed to a severe plugging action which causes most of the flow to go around the particle and the two pillars on either side rather than pushing the particle through the pillar. Because of the inherent unpredictability of this process, the trajectory of such a particle will comprise a seemingly random sequence of upward and downward turns.

To more clearly show the distinctions between these three types of trajectory, we seed particles of the same δ and γ in the same array, i.e., same ϵ, but at different initial locations at the inlet port and observe their positions at the outlet port. We do this by repeating the simulations for 11 different initial positions for particles distributed uniformly along the interpillar gap, and then tracing their centers of mass to the outlet port. The results are shown in Fig. 3. We see in Fig. 3(a) that, for zigzag trajectories, the "span"of these centers of mass remain relatively constant throughout the array. However, for the laterally displaced trajectories in Fig. 3(b), the bumpings against the micropillars result in a collapse of the different initial positions into a single output position, suggesting a "sorted" behavior. Thus, regardless of the initial position along a gap, particles of the same size will be displaced to the same location at the outlet. Finally, the dispersive trajectories in Fig. 3(c) show that the random leftward and rightward motions result in very dispersed output positions, hence the name "dispersive." The "span" of these output positions is very much greater than the span of the input positions. In other words, the dispersive trajectories depend sensitively on their initial conditions. In the future, we would like to quantitatively characterize this sensitivity with Lyapunov exponents and show how this sensitivity, which really is the consequence of the particles exhibiting diffusion of a non-molecular origin, depends on the parameters governing this apparent diffusion.

To further quantify the separation behavior as a function of ϵ, β, η, δ, and γ, we calculate the angular displacement of the trajectories α. To calculate α, we first note the locations where the particle zigzags around micropillars. If we denote the coordinates of the positions of two such consecutive zigzags as (x_1, y_1) and (x_2, y_2), then

$$\alpha = \tan^{-1} \frac{y_2 - y_1}{x_2 - x_1}. \tag{6}$$

(If the particle travels through the array without zigzagging, then we assign $\alpha = \tan^{-1} \epsilon$.) In Fig. 4(a), we plot α as a function of the particle size δ for different values of ϵ at fixed particle deformability γ. We see that for small ϵ, α takes only one of two values with a sharp transition between them. Of these two values, the smaller value of $\alpha \approx 0.1$ corresponds to zigzag trajectories. The zigzag and wrapping of the trajectories around the micropillars result in a small angle of displacement. On the other hand, the higher of the two values of α corresponds to the laterally displaced trajectories. In addition, this high plateau value of α increases as ϵ increases, until a certain threshold around $\epsilon \approx 0.33$ when the value of α begins to fluctuate and is no longer a plateau. This region of fluctuating α is associated with the dispersive trajectories, which allow for a wide range of outlet angles for a given inlet position. We also note that dispersive trajectories are observed not only when particle diameters are comparable to the gap size ($\delta > 0.5$), but also when the row shifts ϵ are

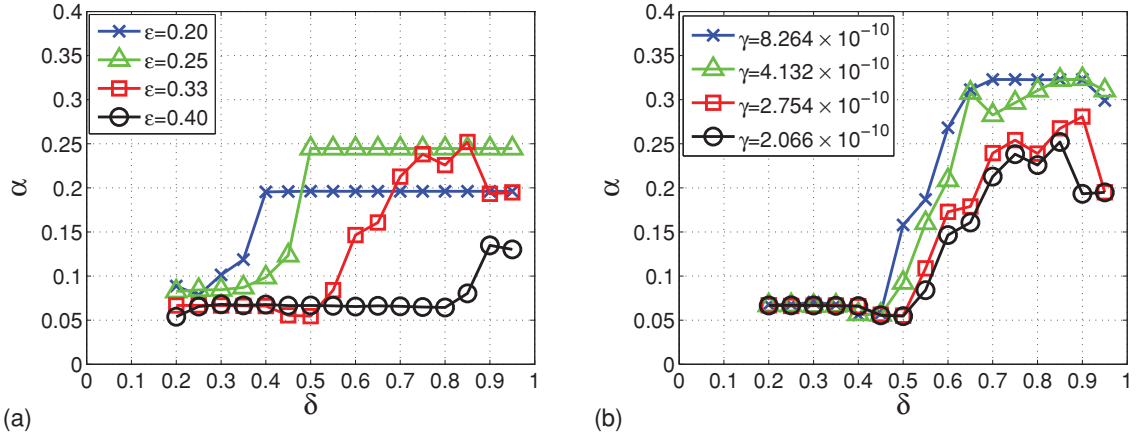

FIG. 4. (Color online) (a) Angular displacement of trajectories α vs dimensionless particle diameter δ for different values of dimensionless lateral row shift in arrangement of micropillars ϵ at fixed dimensionless particle stiffness $\gamma = 2.066 \times 10^{-10}$. (b) Angular displacement α vs dimensionless particle diameter δ for different values of dimensionless particle stiffness γ at fixed dimensionless lateral row shift $\epsilon = 0.33$.

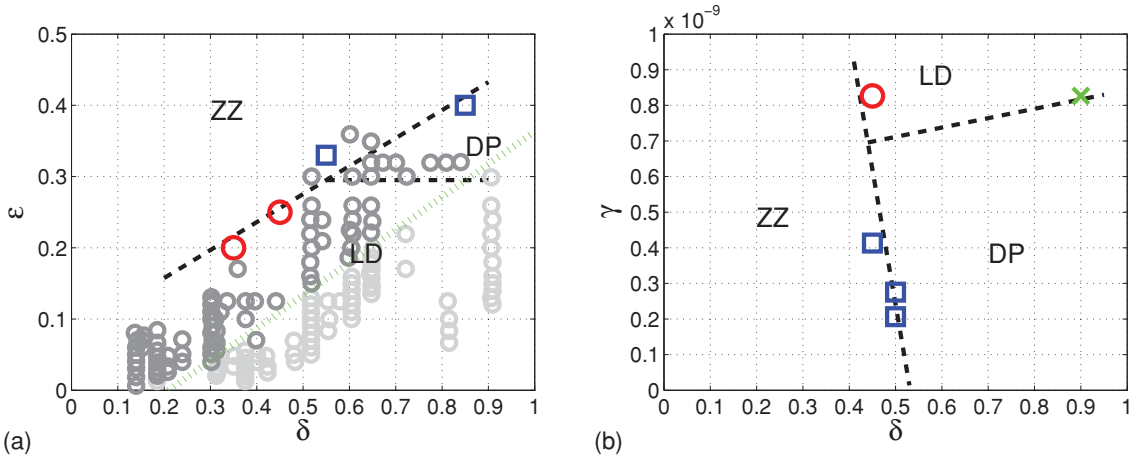

FIG. 5. (Color online) (a) Phase diagram for occurrence of zigzag (ZZ), laterally displaced (LD), or dispersive (DP) trajectories in (δ,ϵ) space. Recall that δ is the dimensionless particle diameter and ϵ is the dimensionless row shift. Large circles (red) denote critical values of δ at $\epsilon = 0.20$ and 0.25 at which ZZ to LD transitions are observed. Large squares (blue) denote critical values of δ at $\epsilon = 0.33$ and 0.40 at which ZZ to DP transitions are observed. In addition, data points from the experiments of Ref. [6] are also plotted: small dark gray circles denote ZZ trajectories, while small light gray circles denote LD trajectories. (b) Phase diagram for occurrence of ZZ, LD, or DP trajectories in (δ,γ) space. The cross (green) denotes critical value of δ at $\gamma = 8.264 \times 10^{-10}$ at which the LD to DP transition is observed. Recall that γ is the dimensionless particle stiffness.

sufficiently large. The reason that small row shifts do not admit dispersive trajectories is that particles tend to glance off the tip of downstream pillars, resulting in minor deflection in their paths. At increasing row shifts, particles increasingly impact the middle of downstream pillars, resulting sometimes in major deflections that cause dispersive trajectories.

From these results, we can sketch a "phase diagram" in (δ,ϵ) space that shows, for a particular value of (δ,ϵ), whether the resulting trajectories are zigzag, laterally displaced, or dispersive. This phase diagram is sketched in Fig. 5(a). A similar phase diagram for rigid particles, obtained experimentally, was available in Ref. [6]. We have included the experimental data points from their phase diagram in Fig. 5(a). We note the discrepancy in our data compared to those from the experiments of Ref. [6], namely that our line separating the region between zigzag trajectories from laterally displaced and dispersive trajectories is shifted leftwards and upward. We suggest that this discrepancy is due to our simulations being two dimensional, which does not account for flow above and below the particles. Therefore, we expect the shear forces acting on the particles to be underestimated in our two-dimensional simulations. In the experiments, the particles will experience higher shear forces. This will in turn modify the flow field surrounding the particles and the particles' trajectories through the array. For example, in our two-dimensional simulations, a particle large enough to plug the gap between adjacent micropillars will cause the fluid to flow around the particle and the micropillars on either side. The particle may remain stationary for a long time, after which a small perturbation will cause it to be bumped off the micropillars, resulting in either a laterally displaced or dispersive trajectory. However, in a three-dimensional scenario, the particle plugging the gap will still permit fluid to flow above and below it. Therefore, the particle may eventually still be able to move through the gap due to the additional shear forces. Therefore, for a given value of (δ,ϵ), the two-dimensional simulations may show lateral displacement or dispersion but the three-dimensional experiments may still show zigzagging.

Interestingly, we also observed that for large enough ϵ, it is possible to transition from zigzag to dispersive trajectories, bypassing lateral displacement. Because dispersive trajectories do not allow the clean separation of particles, they are to be avoided if the application of such devices is for particle separation. Therefore, this observation that there exists regions of "design space" with no lateral displacement has a practical impact on the design of such devices — there exists an upper bound on ϵ necessary for separation, and this upper bound varies with particle size δ and particle stiffness γ.

In practice, these devices have been used to, for example, fractionate whole blood into its components — platelets, red cells, and white cells. Other applications also typically deal with cells. Cells are deformable, but there are no studies on how deformability affects the trajectories of particles as they move through the array. To answer this question, we first calculate the angular displacement α for different particle deformability γ at fixed ϵ. Low values of γ correspond to rigid particles, while increasing γ corresponds to increasing deformability. For example, polystyrene beads with a stiffness of 3 GPa will have $\gamma = 3.79 \times 10^{-12}$, while cells with a characteristic stiffness of 1 kPa will have $\gamma = 1.14 \times 10^{-5}$. In Fig. 4(b), we show how the angular displacement α changes with γ ranging from $\gamma = 0$ to $\gamma = 10^{-9}$. At low γ, we see that α takes only one of two values with a sharp transition between them, corresponding to zigzag and laterally displaced trajectories. As γ is increased, the plateau starts to disappear, to be replaced by fluctuating values, suggesting the onset of dispersive trajectories. From these results, we again sketch a phase diagram in (δ,γ) space in Fig. 5(b). We see that, for the particular value of $\epsilon = 0.33$ used here, the dispersive phase is only observed when $\delta > 0.5$ approximately and $\gamma < 8.264 \times 10^{-10}$ (corresponding to a stiffness greater than 500 MPa) approximately. Since cells typically have stiffness

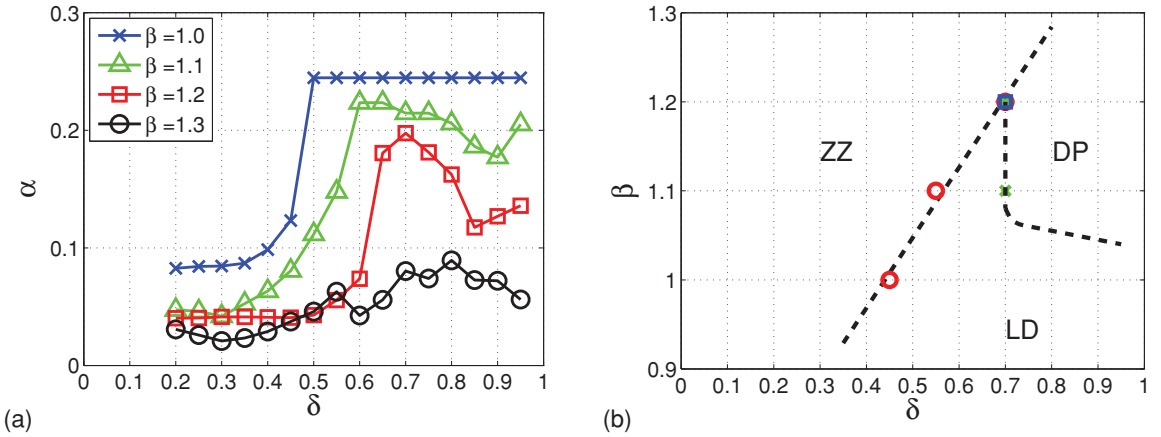

FIG. 6. (Color online) (a) Angular displacement of trajectories α vs dimensionless particle diameter δ for different values of the row separation $\beta = l/\lambda$ at fixed $\epsilon = 0.25$, $\eta = 1$, and $\gamma = 2.066 \times 10^{-10}$. (b) Phase diagram for occurrence of zigzag (ZZ), laterally displaced (LD), or dispersive (DP) trajectories in (δ,β) space.

much less than this threshold value, we therefore do not expect them to exhibit dispersive trajectories. On the other hand, for stiff particles such as polystyrene beads, dispersive trajectories do occur. In fact, we observed again that, for sufficiently large γ (i.e., more deformable or compliant particles), it is possible to transition from zigzag to dispersive trajectories, bypassing lateral displacement. This also places an upper bound on γ in terms of the usefulness of separating stiff or rigid particles.

We also observed in Fig. 4 that, for the zigzag trajectories, the angular displacement α ranges approximately from 0.05 to 0.1 and is not exactly zero. This suggests that the zigzag trajectories have a net sorting behavior (albeit a very small one). When the particles are small, i.e., when δ is small and exhibiting zigzag trajectories, this net sorting behavior reflects the anisotropy of the fluid streamlines with respect to the micropillar array. Therefore, if the separation β between adjacent rows is increased, then the anisotropy of the streamlines is decreased, and α in the zigzag phase should drop to zero. However, for large particles (large δ) or, in general, particles exhibiting laterally displaced trajectories, then there is the possibility that increasing β can result in the particle exhibiting dispersive trajectories instead. In Fig. 6(a), we plot α as a function of particle diameter δ as the row separation β is increased from 1 to 1.3. We see that indeed increasing β results in α approaching zero in the zigzag phase (at small δ). Also, increasing β results in the transition from the laterally displaced phase to the dispersive phase occurring at a much larger δ. The corresponding phase diagram is sketched in Fig. 6(b).

Finally, there is one more parameter to consider, namely, the gap size G between adjacent micropillars in the same row, to see how it affects the trajectories. By varying the dimensionless $\eta = G/\phi$ while keeping all other parameters constant, we see in Fig. 7(a) that increasing η results in a shift toward larger particles to follow the laterally displaced trajectories. We note that the amount of angular displacement α corresponding to the zigzag and laterally displaced trajectories are not changed because the lateral shift ϵ is not changed. The corresponding phase diagram in (δ,η) space is sketched in Fig. 7(b).

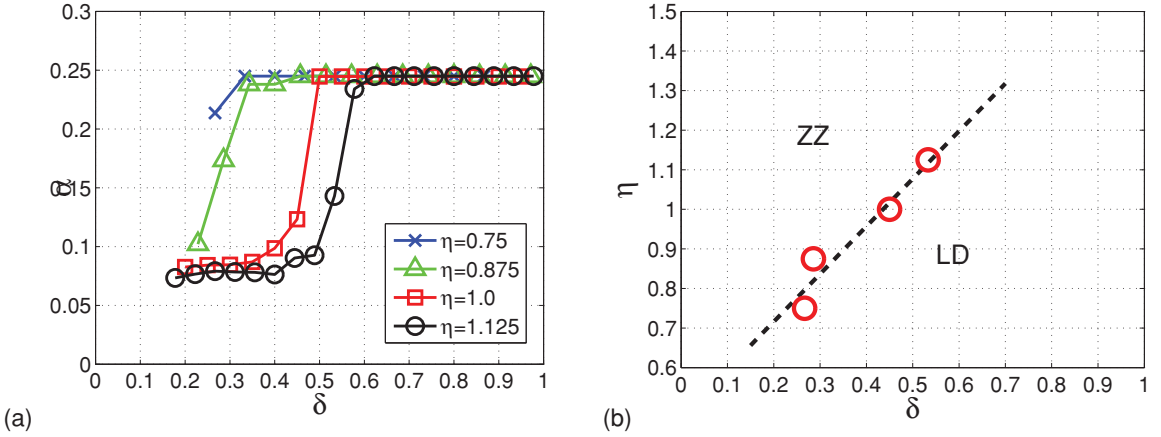

FIG. 7. (Color online) (a) Angular displacement of trajectories α vs dimensionless particle diameter δ for different values of the gap size $\eta = G/\phi$ at fixed $\epsilon = 0.25$, $\beta = 1$, and $\gamma = 2.066 \times 10^{-10}$. (b) Phase diagram for occurrence of zigzag (ZZ) and laterally displaced (LD) trajectories in (δ,η) space.

IV. CONCLUSION

We have used numerical simulations to study the separation of deformable particles in deterministic lateral displacement devices. In particular, we have shown that, in addition to the zigzag and laterally displaced trajectories observed in experiments, the consideration of particle deformability introduces an additional type of trajectory which we call dispersive. We then sketch the regions in phase space, spanned by the row shift, particle diameter, and particle stiffness, in which the different types of trajectories are expected. We have shown that dispersive trajectories are only observed for large (whose diameter is at least half the interpillar gap distance) and rigid particles (whose stiffness is greater than 500 MPa). We have shown that, in this phase space, there are transitions from zigzag to dispersive trajectories, bypassing lateral displacement. This is undesirable experimentally because it limits the ability of the device to separate particles according to size.

In the future, we plan to extend our numerical simulations to studying the feasibility of separating polymers rather than particles in such devices [14].

ACKNOWLEDGMENTS

We thank Howard A. Stone for insightful discussions.

[1] L. Huang, E. Cox, R. Austin, and J. Sturm, Science **304**, 987 (2004).
[2] J. Davis, D. Inglis, K. Morton, D. Lawrence, L. Huang, S. Chou, J. Sturm, and R. Austin, Proc. Natl. Acad. Sci. USA **103**, 14779 (2006).
[3] J. Green, M. Radisic, and S. Murthy, Anal. Chem. **81**, 9178 (2009).
[4] D. Inglis, J. Davis, T. Zieziulewicz, D. Lawrence, R. Austin, and J. Sturm, J. Immunol. Methods **329**, 151 (2008).
[5] K. Morton, K. Loutherback, D. Inglis, O. Tsui, J. Sturm, S. Chou, and R. Austin, Lab on a Chip **8**, 1448 (2008).
[6] D. Inglis, J. Davis, R. Austin, and J. Sturm, Lab Chip **6**, 655 (2006).
[7] J. Koplik and G. Drazer, Phys. Fluids **22**, 052005 (2010).
[8] H. Deuling and W. Helfrich, Biophys. J. **16**, 861 (1976).
[9] T. Fischer, C. Haest, M. Stöhr-Liesen, H. Schmid-Schönbein, and R. Skalak, Biophys. J. **34**, 409 (1981).
[10] K. Loutherback, K. Chou, J. Newman, J. Puchalla, and R. Austin, and J. Sturm, Microfluid. Nanofluid. **9**, 1143 (2010).
[11] M. Heller and H. Bruus, J. Micromech. Microeng. **18**, 075030 (2008).
[12] C. Peskin, Acta Numerica **11**, 479 (2002).
[13] D. Le, B. Khoo, and K. Lim, Comput. Methods Appl. Mech. Eng. **197**, 2119 (2008).
[14] J. Ou, J. Cho, D. W. Olson, and K. D. Dorfman, Phys. Rev. E **79**, 061904 (2009).